

# A study of the construction of the correlation matrix of $^{241}\text{Pu}(\text{nth},\text{f})$ isobaric fission yields

Sylvain Julien-Laferrrière<sup>1,2,\*</sup>, Abdelaziz Chebboubi<sup>1</sup>, Grégoire Kessedjian<sup>2</sup>, and Olivier Serot<sup>1</sup>

<sup>1</sup> CEA, DEN, DER, SPRC, 13108 Saint-Paul-Lez-Durance, France

<sup>2</sup> LPSC, Université Grenoble-Alpes, CNRS/IN2P3, 38026 Grenoble, France

Received: 6 December 2017 / Received in final form: 20 March 2018 / Accepted: 25 May 2018

**Abstract.** Two blind analyses for  $^{241}\text{Pu}(\text{nth},\text{f})$  isobaric fission yields have been conducted, one analysis using a mix of a Monte-Carlo and an analytical method, the other one relying only on analytical calculations. The calculations have been derived from the same analysis path and experimental data, obtained on the LOHENGRIN mass spectrometer at the Institut Laue-Langevin. The comparison between the two analyses put into lights several biases and limits of each analysis and gives a comprehensive vision on the construction of the correlation matrix. It gives confidence in the analysis scheme used for the determination of the fission yields and their correlation matrix.

## 1 Introduction

Nuclear fission yields are key parameters for understanding the fission process [1] and to evaluate reactor physics quantities, such as decay heat [2]. Despite a sustained effort allocated to fission yields measurements and code development, the recent evaluated libraries (JEFF-3.3 [3], ENDF/B-VII.1 [4],...) still present shortcomings, especially in the reduction of the uncertainties and the presence of reliable variance-covariance matrices. Yet these matrices are compulsory to use nuclear data, in particular when it comes to propagate uncertainties. A collaboration among the French Alternative Energies and Atomic Energy Commission (CEA), the Laboratory of Subatomic Physics and Cosmology (LPSC) and the Institut Laue-Langevin (ILL), started in 2009, aims at tackling these issues by providing precise measurements of fission yields with the related experimental covariance matrices for major actinides [5]. In particular for the  $^{241}\text{Pu}$  nuclide which is a major isotope in the context of multi-recycling and which is investigated in the present work.

Two measurements for thermal neutron induced fission of  $^{241}\text{Pu}$  have been carried out at the ILL in Grenoble (France), using the LOHENGRIN mass spectrometer [6,7] in May 2013 [8], labelled as Exp.1, and November 2015 [9], labelled as Exp.2. This instrument allows a selection of fission products regarding the  $A/q$  and  $E_k/q$  ratios, supplying an ion beam of mass  $A$ , kinetic energy  $E_k$  and of ionic charge  $q$  with an excellent mass resolution

( $\Delta A/A \simeq 1/400$ ). A double ionization chamber with a Frisch grid, similar to the one used in [10], is used to measure the count rate  $N(A, t, E_k, q)$ . The entire heavy peak region has been measured as well as a significant number of light masses.

The analysis scheme for the high yields region<sup>1</sup> (85–111 for the light masses and 130–151 for the heavy masses) has been subjected to two independent blind analyses [11], from the same raw data and analysis scheme.

The first one relies on a Monte-Carlo (MC) approach coupled with analytical calculations while the second one is based on a full analytical procedure. The main difference stands in the uncertainties propagation. In the analytical approach, for each step of the analysis, each parameter is supposed to have a Gaussian distribution. A classic approach is adopted, where functions are linearised by approximation to the first-order Taylor series expansion. On the contrary, in MC, no approximation is made when propagating uncertainties. The initial count rates are randomly generated from a Gaussian distribution with a large number of MC events. The mean value, standard deviation and covariances for each step are computed directly from the probability density functions.

The goal of this work is to unveil the biases and limits of each method and see if they lead to similar results despite the hypothesis made. If not, these biases shall be understood and controlled. This gives confidence in the

\* e-mail: [julienl@lpsc.in2p3.fr](mailto:julienl@lpsc.in2p3.fr)

<sup>1</sup> For the low yields regions (symmetric and very asymmetric masses), the analysis procedure is different due to a contamination phenomenon that will not be presented here.

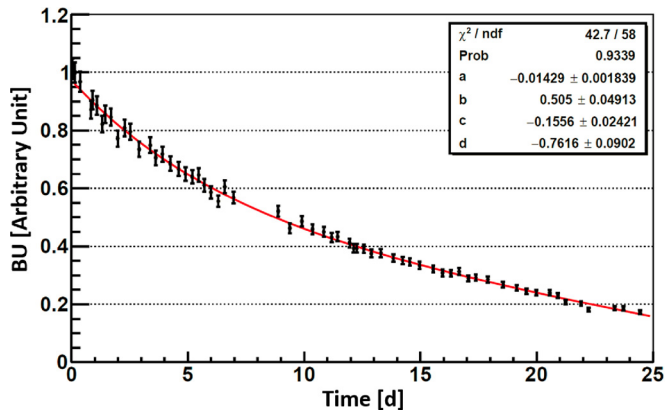


**Fig. 1.** The time evolution of the amount of fissile material in the target, so-called Burn-Up ( $BU$ ) for Exp.2. The experimental points, in black, fitted by equation (2), in red.

analysis path adopted while understanding the important steps of the analysis in particular in the construction of the covariance matrix.

At first, the analysis procedure from the raw  $N(A, t, E_k, q)$  data to the determination of the isobaric yields  $Y(A)$  will be presented in Section 2. Then the two methods will be compared in particular the experimental correlation matrices, and the important steps of this analysis will be underlined, in Section 3.

## 2 Analysis path

The analysis path followed by both MC and analytical approaches is described in this section.

The raw data obtained from the experiments, at time  $t$ , are the count rates  $N(A, t, E_k, q)$  for a mass  $A$ , at a kinetic energy  $E_k$  and at the ionic charge state  $q$ . These count rates are considered as independent from each other since only the statistical uncertainty is accounted for. The definition of the total count rate for the mass  $A$  is:

$$N(A) = \int_{E_k} \sum_q \frac{N(A, t, E_k, q)}{BU(t)} dE_k, \quad (1)$$

where the Burn-Up,  $BU$ , is the relative estimation over time,  $t$ , of the amount of fissile material in the  $^{241}\text{Pu}$  target used for the experiments (see for example Fig. 1). The time evolution of the  $BU$  is carefully estimated by regularly measuring the overall ionic charge and kinetic energy distribution of mass 136, since it corresponds experimentally to an optimal count rate and mass separation. It is a mandatory normalization step since the amount of fissile material is constantly decreasing over time due to the nuclear reactions consuming the  $^{241}\text{Pu}$  and the loss of material because of the harsh environmental conditions of the target [12]. The  $BU$  also takes into account the ion beam fluctuations over time as well as the incident neutron flux variations. Additional details on the procedure used for the  $BU$  measurement can be found in [13]. The  $BU$  points are fitted in order to be extrapolated to the measurement times. No theoretical consideration is taken for the choice of the fit function due to the complexity of physical

phenomena governing the target behaviour. For the Exp.2 for example, the  $BU$  behaviour is well reproduced by the sum of a polynomial of 1st order and an exponential function, as seen in Figure 1:

$$BU(t) = a \cdot t + b + \exp(c \cdot t + d). \quad (2)$$

Since the beam time is limited, the complete  $(E_k, q)$  distribution for each mass cannot be measured. The experimental method, refined over time [8,14,15], is to transform the sum over the ionic charge states into a division by the probability density function of the ionic charge states  $P(q)$ , and the integral over the kinetic energies into a summation over bins of a constant step. Equation (1) becomes:

$$N_{q_i}(A) = \sum_{E_k} \frac{N(A, t, E_k, q_i)}{P(q_i) \cdot BU(t)}. \quad (3)$$

One scan of the ionic charge states distribution at a constant kinetic energy is made for each mass and at least three scans of the kinetic energy distribution at different ionic charge states. Thanks to this, the ionic charge distribution  $P(q)$  can be estimated and at least three different values of the same  $N(A)$  are obtained:  $N_{q_1}(A)$ ,  $N_{q_2}(A)$  and  $N_{q_3}(A)$ , one for each measured kinetic energy distribution. To properly expressed  $N_{q_i}(A)$ , one should take into account the existing correlation between the kinetic energy and ionic charge distributions [8,15]. To simplify the comparison proposed in this work, this step has been by-passed.

If the three estimations of the same  $N(A)$  are compatible, the mean value  $\bar{N}(A)$  taking into account the experimental covariance matrix,  $\mathbf{C} \in \mathcal{M}_n(\mathbb{R})$ , is extracted by minimizing the generalized  $\chi^2$  [16]:

$$\bar{N}(A) = \left( \sum_{i,j}^{n,n} (C^{-1})_{i,j} \right)^{-1} \left( \sum_{i,j}^{n,n} (C^{-1})_{i,j} \cdot N_{q_j}(A) \right), \quad (4)$$

with a reduced variance:

$$\text{Var}(\bar{N}(A)) = \left( \sum_{i,j}^{n,n} (C^{-1})_{i,j} \right)^{-1}, \quad (5)$$

where  $n$  is the number of energy scans for the mass  $A$ . How  $\mathbf{C}$  is obtained will be detailed in the Section 3.1. The compatibility is checked through a generalized  $\chi^2$  test taking into account the experimental covariances between the  $N(A)$ 's, such as the  $p$ -value is above 90% of confidence level:

$$\chi^2(\bar{N}(A)) = \sum_i^n \sum_j^n (N_{q_i}(A) - \bar{N}(A)) C_{i,j}^{-1} (N_{q_j}(A) - \bar{N}(A)). \quad (6)$$

When this criterion is not met, an additional independent uncertainty,  $\delta$ , is incrementally added to the diagonal of the covariance matrix  $\mathbf{C}$  of the  $N(A)$ 's, see equation (7), until a satisfying  $\chi^2$  is reached. This additional independent

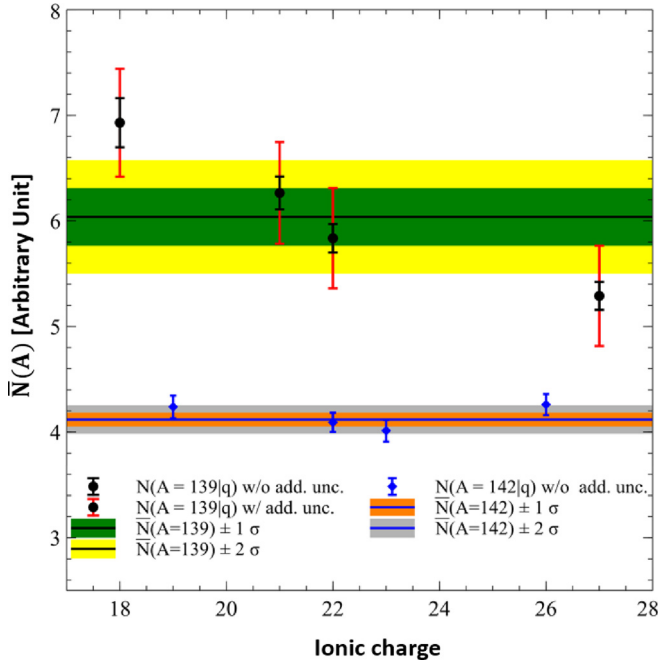


**Fig. 2.** Each  $N_{q_i}(A)$  and their mean value  $\bar{N}(A)$  for the masses 139 and 142. The compatibility criteria are met for  $A=142$  while additional uncertainties (add. unc.) are needed for  $A=139$ .

uncertainty is accounting for the  $N(A)$ 's dispersion due to the flawed control of the instrument.

$$C_{ii}(k) = C_{ii}(0) + k \cdot \delta, \quad (7)$$

where  $k$  is the number of increments. This process is illustrated in Figure 2.

As already specified in the introduction, two sets of experiments have been used in this analysis, the first one measured in May 2013, Exp.1, and the second one in November 2015, Exp.2. Since the experimental environment is different from one experience to the other (neutron flux, target, etc,...) the two sets are considered as independent even though both are obtained on the LOHENGRIN mass spectrometer. The next step is thus to combine these two experiments to obtain the merged vector  $\bar{N}(A)_{\text{mgd}}$  (mgd stands for merged), by doing a relative normalization of one set to the other, relying on the value of the  $\bar{N}(A)$  obtained for the 14 common masses, see Table 1.

If  $\mathbf{X}$  and  $\mathbf{Y}$  are respectively the  $\bar{N}(A)$  vectors for the common masses of Exp.1 and Exp.2, then, to normalize Exp.1 with respect to Exp.2, one has to minimize the residual vector  $\varepsilon$ :

$$\varepsilon = \mathbf{Y} - \kappa \cdot \mathbf{X}. \quad (8)$$

The best estimator of  $\kappa$  is the normalization factor  $k$  of Exp.1 with respect to Exp.2, obtained through the generalized least square method, in its matrix form [17]:

$$k = (\mathbf{X}^T \boldsymbol{\Omega}^{-1} \mathbf{X})^{-1} \mathbf{X}^T \boldsymbol{\Omega}^{-1} \mathbf{Y}, \quad (9)$$

where  $\boldsymbol{\Omega}$  is the combined covariance matrix for Exp.1 and Exp.2, taken to be  $\boldsymbol{\Omega} = \boldsymbol{\Omega}_X + \boldsymbol{\Omega}_Y$ . Eventually, the mean values of the normalized set of the two experiments are extracted for the common masses in a similar way to equation (4).

The last step is the absolute normalization to obtain the yields,  $Y(A)$ . Ideally, this normalization is done by taking  $\sum_{i \in H} \bar{N}(A_i)_{\text{mgd}} = 1$ ,  $H$  being the masses of the heavy peak. This is true for pre-neutron yields when the contribution of ternary fission is not taken into account. In our experiments, post-neutron yields from the masses 121 to 159 are obtained. The sum of the mass yields for  $A > 159$  represents 0.26% in JEFF-3.3 of the heavy peak and 0.03% for ENDF/B-VII.1. For the normalization step, a conservative uncertainty of 0.5% is taken, accounting for the absence of the very heavy masses,  $A > 159$  and the approximation that the sum over the heavy masses is equal to 1 for post-neutron yields.

However, since this document is only focused on high yields, the completeness of the  $Y(A)$  distribution for the heavy masses is not satisfyingly achieved. Nonetheless, in the scope of this document, the normalization will be done as previously explained, in order to discuss the impact of the absolute normalization.

## Summary

The analysis path can be summarized in the following steps:

- (1) sum over the kinetic energy distribution:  $N(A, t, q_i) = \sum_{E_k} N(A, t, E_k, q_i)$ ;
- (2) determine the  $P(q)$  distribution and divide step (1) by  $P(q_i)$ :  $N_{q_i}(A, t) = \sum_{E_k} \frac{N(A, t, E_k, q_i)}{P(q_i)}$ ;
- (3) evaluate the  $BU$  at  $t$  and divide step (2) by  $BU(t)$ :  $N_{q_i}(A) = \sum_{E_k} \frac{N(A, t, E_k, q_i)}{P(q_i) \cdot BU(t)}$ ;
- (4) compute the mean value for each mass with eventual additional uncertainties:  $\bar{N}(A)$ ;
- (5) normalize (relative normalization) and merge the two sets of experiments:  $\bar{N}(A)_{\text{mgd}}$ ;
- (6) process the absolute normalization:  $Y(A)$ .

## 3 Covariance matrices comparison

### 3.1 Differences between Monte-Carlo and analytical methods

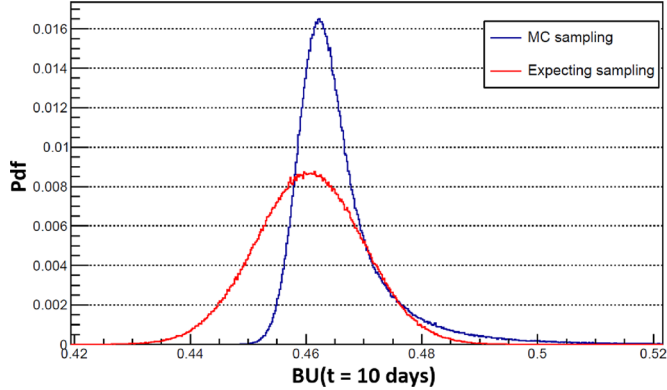
In the MC method, all count rates are sampled from a Poisson law. In order to assess  $BU(t)$ , the fitted  $BU$  parameters are first decorrelated and then sampled from a Gaussian law with a unit standard deviation. The decorrelation is obtained through the equation (10) [18]:

$$\mathbf{S} = \boldsymbol{\Omega}_R^{-1/2} \mathbf{R} \quad (10)$$

with  $\mathbf{R}$  is the fitted parameters,  $\mathbf{S}$  the free parameters and  $\boldsymbol{\Omega}_R$  is the covariance matrix of the fitted parameters. However, when the  $BU$  is computed from the sampling of the uncorrelated fit parameters, the probability density function obtained is no more a Gaussian distribution, see Figure 3. In the analytic method, when propagating uncertainties each parameter is supposed to have a Gaussian distribution, if it is not the case the biases of

**Table 1.** Set of masses measured in the two experiments and masses common to the two experiments.

Exp.1	Exp.2	Common masses
130–151	85, 90, 92, 93, 94, 96, 98, 100–109, 111, 130, 133–142, 146, 147, 149	130, 133–142, 146, 147, 149

**Fig. 3.** The probability density function of the MC sampling for the value of the  $BU$  at  $t = 10$  days for Exp.2, in blue, compared to the expected Gaussian, in red.

this hypothesis should be controlled. This issue is under investigation. In order to still be able to compare the two analyses for the next steps, in the present work, the propagation of the  $BU$  uncertainties by the MC method is achieved analytically.

The covariance between  $N(A)$ 's, used in equation (4), can be decomposed between the covariances induced by the  $BU$  and the statistical covariances:

$$\mathbf{C} = \mathbf{Cov}(N_{q_k}(A_i), N_{q_l}(A_j)) = \mathbf{Cov}_{\text{stat}} + \mathbf{Cov}_{BU}, \quad (11)$$

Only covariance at the step (2) is computed through MC as expressed by equation (12), with  $m$  the MC event and  $N_{q_k}(A_i, t)$  the arithmetic mean value of the  $N_{q_k}^m(A_i, t)$ 's.  $\mathbf{Cov}_{\text{stat}}$ , the statistical part of the covariance matrix is then defined as follows:

$$\begin{aligned} & \mathbf{Cov}_{\text{stat}}(N_{q_k}(A_i, t), N_{q_l}(A_j, t')) \\ &= \sum_m (N_{q_k}^m(A_i, t) - N_{q_k}(A_i, t))(N_{q_l}^m(A_j, t') - N_{q_l}(A_j, t')), \end{aligned} \quad (12)$$

where  $t$  and  $t'$  are respectively the times at which the mass  $A_i$  at the ionic charge state  $q_k$  and the mass  $A_j$  at the ionic charge state  $q_l$  have been measured. In the analytic case, equation (12) is written as equation (13):

$$\begin{aligned} & \mathbf{Cov}_{\text{stat}}(N_{q_k}(A_i, t), N_{q_l}(A_j, t')) \\ &= \frac{N_{q_k}(A_i, t)N_{q_l}(A_j, t')}{P_{q_k}(A_i)P_{q_l}(A_j)} \times \mathbf{Cov}(P_{q_k}(A_i), P_{q_l}(A_j)), \end{aligned} \quad (13)$$

where  $\mathbf{Cov}(P_{q_k}(A_i), P_{q_l}(A_j))$  is the covariance coming from the ionic charge distribution. Therefore if  $A_i \neq A_j$ , this term is null. Otherwise by propagating in a classical way the covariance, it is written:

$$\begin{aligned} \mathbf{Cov}(P_{q_k}(A_i), P_{q_l}(A_j)) &= \frac{P_k^2 P_l^2}{I_k^2 I_l^2} \\ &\times \left( (I_{\text{tot}} - I_k)(I_{\text{tot}} - I_l) \mathbf{Cov}(I_k, I_l) \right. \\ &\quad - (I_{\text{tot}} - I_k) I_l \sum_{m \neq l} \mathbf{Cov}(I_k, I_m) \\ &\quad - (I_{\text{tot}} - I_l) I_k \sum_{n \neq k} \mathbf{Cov}(I_n, I_l) \\ &\quad \left. + I_k I_l \sum_{m \neq l} \sum_{n \neq k} \mathbf{Cov}(I_m, I_n) \right), \end{aligned} \quad (14)$$

with  $I_k$  the count rates of the charge  $k$ ,  $I_{\text{tot}} = \sum_k I_k$  the total count rate of the ionic charge distribution, and  $P_k = \frac{I_k}{I_{\text{tot}}}$  the normalized count rate. One has to note, since each measurement is independent, that only the diagonal of the covariance matrix of the count rate is not null.

The  $BU$  correlation is taken into account analytically in both analyses through:

$$\mathbf{Cov}_{BU}(N_{q_k}(A_i), N_{q_l}(A_j)) = \frac{N_{q_k}(A_i)N_{q_l}(A_j)}{BU_{ik}BU_{jl}} \mathbf{Cov}(BU_{ik}, BU_{jl}), \quad (15)$$

with,

$$\mathbf{Cov}(BU_{ik}, BU_{jl}) = \sum_m \sum_n \frac{\partial BU_{ik}}{\partial r_m} \frac{\partial BU_{jl}}{\partial r_n} \mathbf{Cov}(r_m, r_n), \quad (16)$$

where  $\{r_k\}$  are the  $BU$  parameters. As a consequence, for the analysis using MC, the following steps, (4–6), have to be computed analytically.

A final difference can be underlined. For independent parameters, the MC induces small correlations, even for pseudo-random numbers generated by different seeds. Since these correlations are low compared to the real experimental correlations, it is not an issue. It is worth noting that this MC numerical correlation artefact is dependent on the number of MC events. In this work, for  $10^5$  events, the order of magnitude of this correlation artefact is  $10^{-5}$ .

### 3.2 Step (3): impact of the $BU$ on correlations

The  $BU$  is at this stage the only source of inter-masses correlations. To illustrate this, a mean experimental time  $\bar{t}(A)$  has been constructed for each mass.  $\bar{t}(A)$  is the mean time at which the mass  $A$  is measured.

In Figure 4, one can see that masses having close experimental time have high correlation and vice versa. For example, the masses 100–109 (black circle) have been measured very closely in time, the same goes for the masses 138–141 (green circle). The correlations in these groups are very high, whereas inter groups correlations are close to 0.

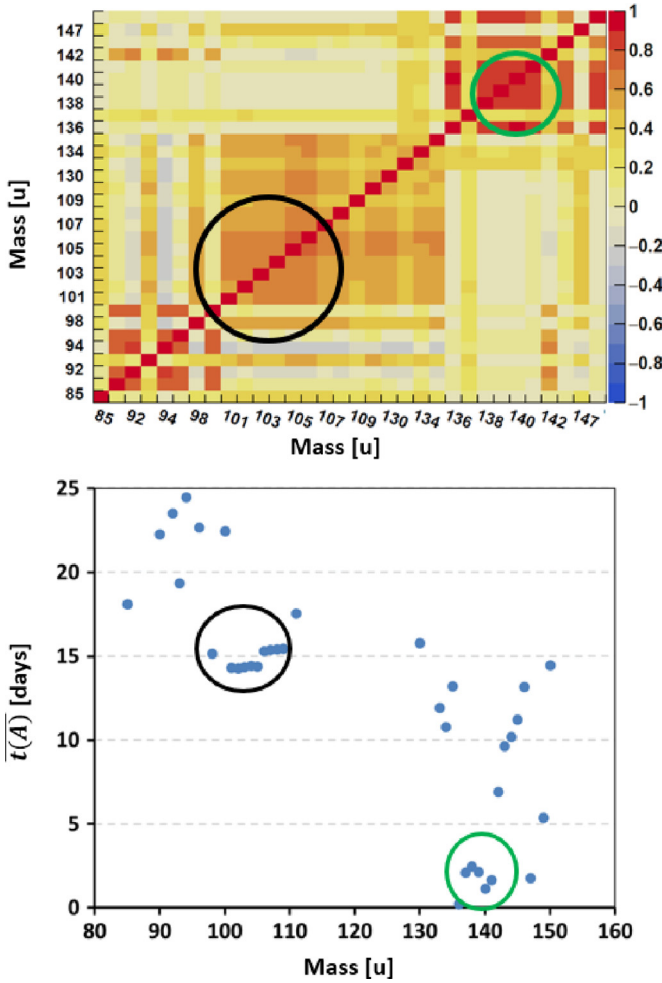


**Fig. 4.** The correlations obtained in the analysis procedure for the  $\bar{N}(A)$  for Exp.2, on the top, and the mean experimental time for each mass, on the bottom. Masses done at close experimental times (for example the masses in black or green circles) have high correlations and vice versa.

The correlations obtained at this stage for the mix MC and analytic and the analytic methods are very similar, the highest absolute difference observed in the correlation matrix is  $\Delta \text{Corr} = 0.0032$  which represents a relative difference of  $\frac{\Delta \text{Corr}}{\text{Corr}} = 1.3\%$ , see [Figure 5](#).

### 3.3 Step (4): impact of the additional dispersion uncertainties

As it has just been explained, the correlation matrix is at this stage governed by the *BU*. The additional dispersion uncertainties introduced after equation (6), as independent uncertainties, wash away the initial structures. The weight of the common uncertainties coming from the *BU* is reduced.

The impact of these additional uncertainties are shown in [Figures 6 and 7](#).

### 3.4 Step (5): impact of the relative normalization

The definition of the relative normalization factor  $k$ , in equation (9), is dependent on which experiment is the reference. Both the out-coming  $\bar{N}(A)_{\text{mgd}}$  and the

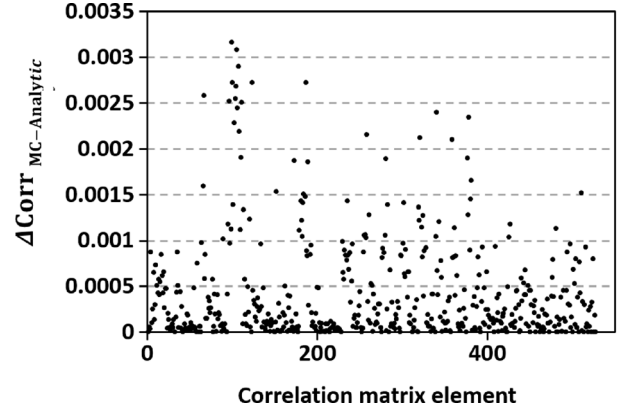


**Fig. 5.** The absolute difference in the correlation matrix between the two analyses at step (3).

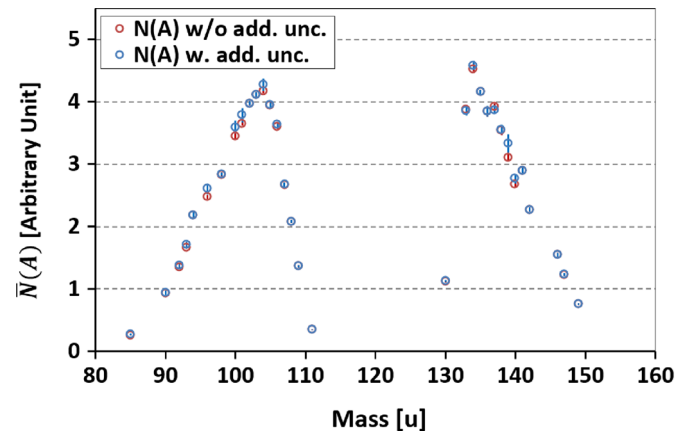


**Fig. 6.** The  $\bar{N}(A)$  distribution with (in blue) and without (in red) the additional dispersion uncertainties (add. unc.) for Exp.2.

associated correlation matrix will be affected, as it can be observed from [Figures 8 and 9](#). Indeed, if Exp.1 is normalized with respect to Exp.2, the variance of  $\mathbf{Z} = k\mathbf{X}$ , the normalized vector of  $\mathbf{X}$ , will be increased by the normalization, while the variance of  $\mathbf{Y}$  remains constant.

Ultimately, when the mean value for the common masses of  $\mathbf{Y}$  and  $\mathbf{Z}$  is computed similarly to equation (4), taking into account the covariance matrices,  $\bar{N}(A)_{\text{mgd}}$  depends on the experiment considered as the reference. As it can be seen in [Figure 8](#), Exp.2 has initially smaller uncertainties. When it is the reference, the uncertainties after normalization are considerably smaller since they are monitored by Exp.2 uncertainties. On the contrary, mean values are barely sensitive to which reference is chosen.

In order to choose the reference, the cumulative eigenvalues of the correlation matrix is plotted in [Figure 10](#). A first approach is to consider that a smooth increase of the cumulative eigenvalue is preferable. It means each mass brings a significant amount of information. The information is well spread between the different measurements and the correlation matrix is less structured. Considering this approach, the Exp.2 is taken as reference for the rest of this work. Work is in progress in order to construct an observable quantifying the quality of the information depending on the reference, similarly to the work presented in [19].

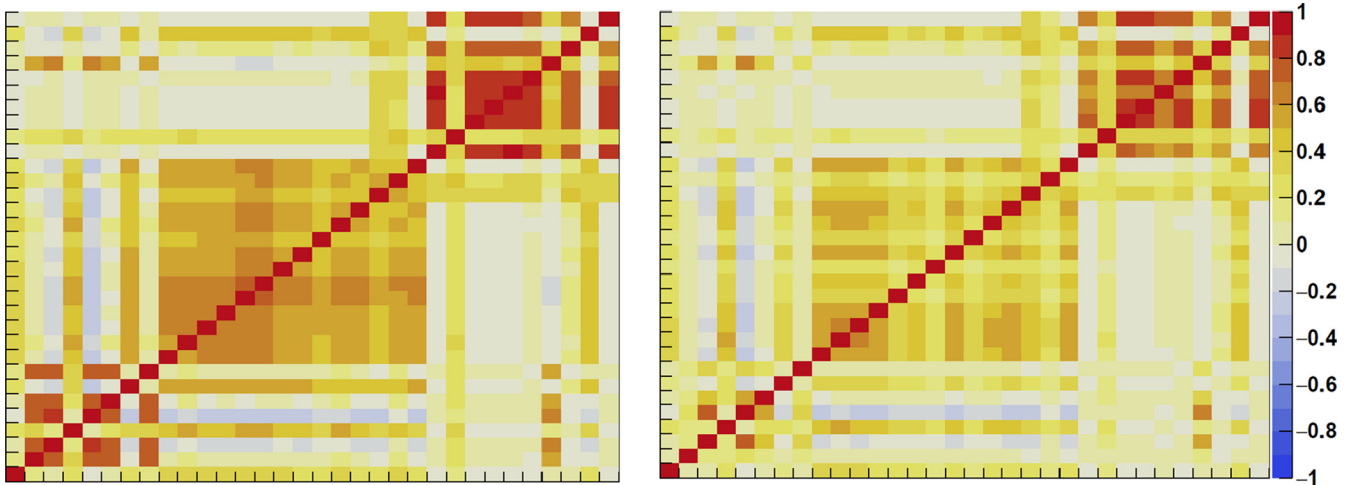


**Fig. 7.** The correlation matrix, for Exp.2, of the  $\bar{N}(A)$  without the additional dispersion uncertainties, on the left, and with, on the right. X and Y labels are identical to [Figure 4](#) (top).

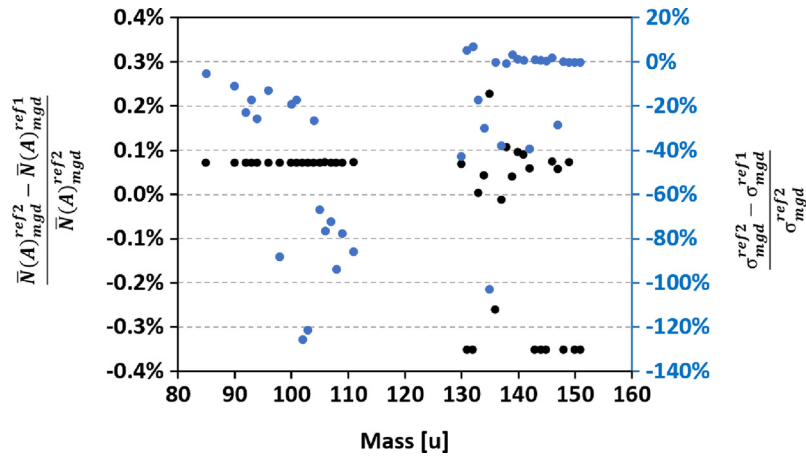


**Fig. 8.** The relative difference on  $\bar{N}(A)_{\text{mgd}}$  in black on the left axis, and on the uncertainty  $\sigma_{\text{mgd}}$  in blue on the right axis, when the reference is Exp.1 or Exp.2. For the sake of the comparison, both sets of  $\bar{N}(A)_{\text{mgd}}$  have been normalized to 1.

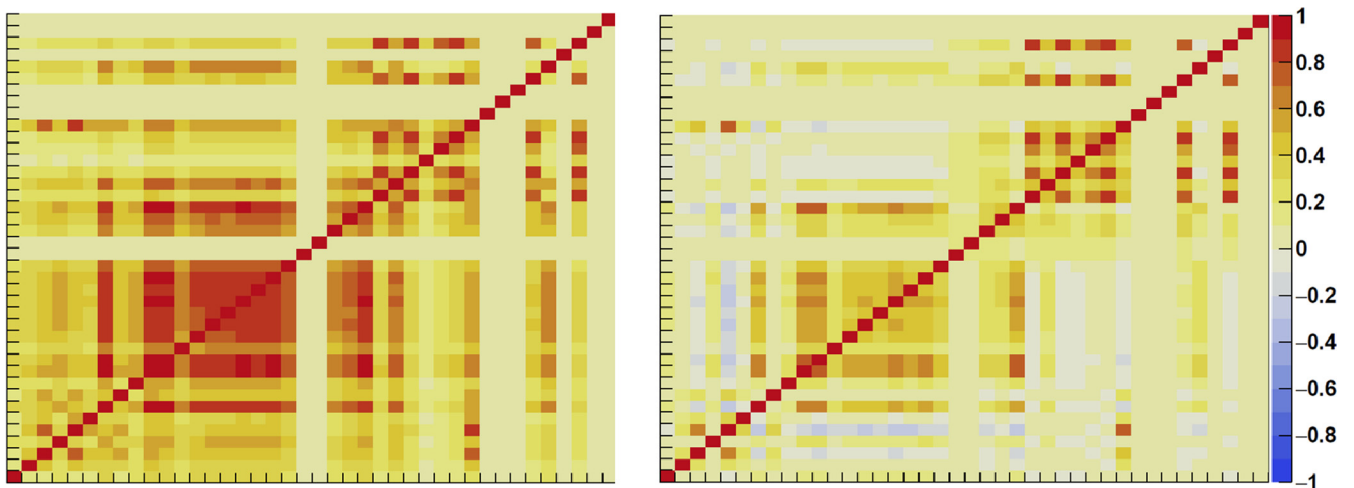


**Fig. 9.** The correlation matrix after the relative normalization when Exp.1 is the reference, on the left, and when Exp.2 is the reference, on the right. X and Y labels are identical to [Figure 12](#) (top).

A new analysis of the 2013 data is in progress and is expected to give results with lower uncertainties. In that case, it is expected that the choice of the reference has a reduced impact.

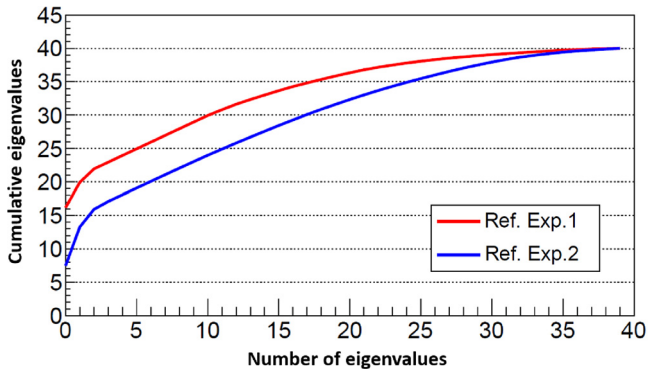


**Fig. 10.** The cumulative eigenvalues of the correlation matrix of the  $\bar{N}(A)$  for the Exp.1 in blue and the Exp.2 in red.

### 3.5 Step (6): impact of the absolute normalization

The impact on the  $Y(A)$  correlation matrix of the absolute normalization is illustrated in Figure 11. In Figure 11, a diagonal correlation matrix is displayed (top left), while the analytic  $^{241}\text{Pu}(\text{nth},\text{f})$  experimental  $\bar{N}(A)_{\text{mgd}}$  correlation matrix is shown (bottom left). On the right, the correlation matrices after the absolute normalization depending on which is the input correlation matrix. Thus, the effect of the absolute normalization step alone is shown on the top right of Figure 11. The  $Y(A)$  correlation matrix (bottom right) is the combination of the effect of the absolute normalization alone and the experimental  $\bar{N}(A)_{\text{mgd}}$  correlation matrix (bottom left).

The  $Y(A)$  correlation matrix structure is marked by the normalization procedure that creates a correlation background.

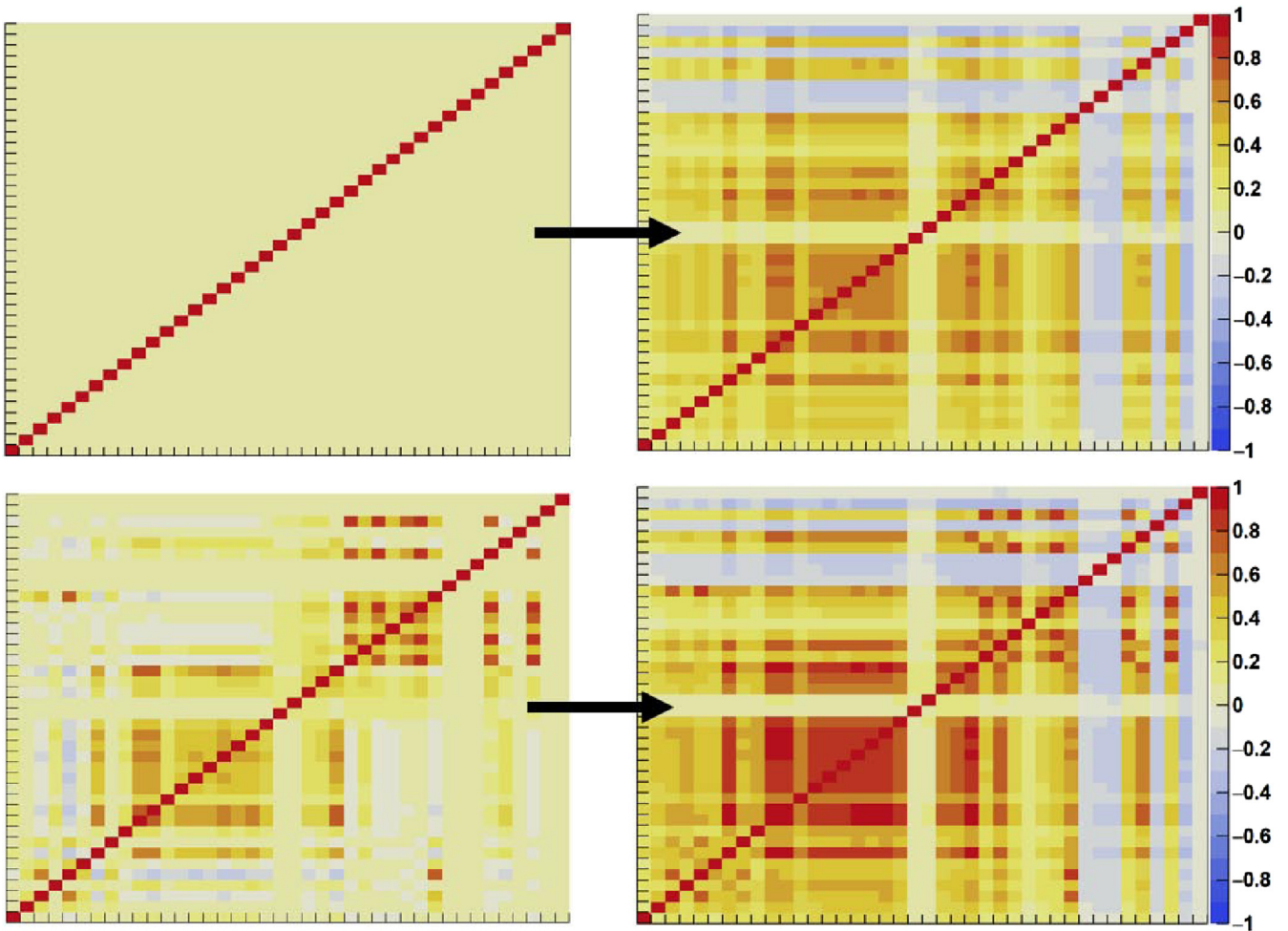


**Fig. 11.** On top, the correlation matrix of the  $\bar{N}(A)_{\text{mgd}}$  if inter-masses correlations are set to 0 (left) and its propagation through the absolute normalization (right). On the bottom, the  $\bar{N}(A)_{\text{mgd}}$  analytic correlation matrix (left) and its propagation through the absolute normalization (right). The analytic  $Y(A)$  correlation matrix (bottom right) is a combination of the effect of the normalization alone (top right) and the initial  $\bar{N}(A)_{\text{mgd}}$  analytic correlation matrix (bottom left).  $X$  and  $Y$  labels are identical to Figure 12 (top).

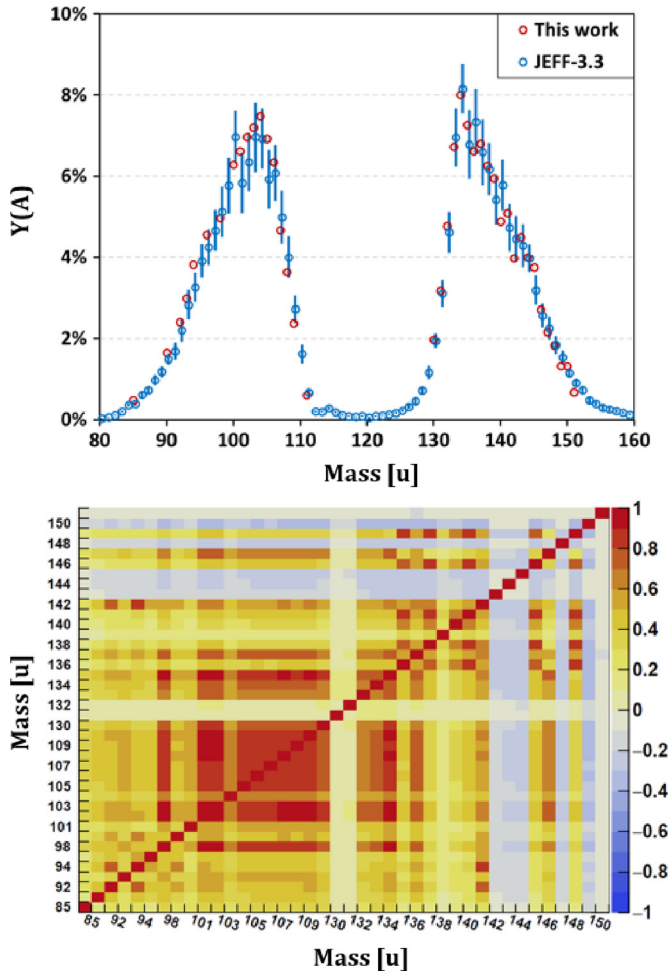


**Fig. 12.** The  $Y(A)$  for  $^{241}\text{Pu}(\text{nth},f)$  and their uncertainties (at  $1\sigma$ ) obtained (in red), compared to JEFF-3.3 (in blue). On the bottom, the  $Y(A)$  experimental correlation matrix.

## 4 Conclusion and perspectives

The experimental  $Y(A)$  obtained in this work is presented in Figure 12 and compared to JEFF-3.3. The precision achieved in this experimental work is much better than the JEFF-3.3 evaluation and significant discrepancies are observed, in particular in the light masses.

An effect not taken into account in this work is the correlation between the kinetic energy and ionic charge distributions. Since the ionic charge scan is made at a specific kinetic energy,  $E_k$ , this correlation has to be taken into account in order to properly estimate  $P(q_i)$  in equation (3) [20]. This is expected to significantly reduce the need of the additional dispersion uncertainties from Section 3.3.

This work showed that both analyses give identical results for the estimation of the correlations matrix when the MC bias highlighted during the  $BU$  sampling step is bypassed. The  $BU$  sampling bias is under investigation in order to compare the MC and analytic methods on the full analysis scheme and not only on steps (1–3). For every

steps of the analysis scheme, the correlation matrices obtained by the two different analyses have been compared and no larger differences than the one observed at step (3) are seen, giving a strong confidence in our method. Mean values and uncertainties are also identical, validating both analyses. The structure of the correlation matrix is well understood, the importance of several steps in the construction of the correlation matrix have been emphasized: the  $BU$  creates strong positive correlations while the additional uncertainties due to the limits of the experimental method flatten the correlation matrix. Finally the absolute normalization creates a correlation background.

The analyses have been compared without the correlation between the kinetic energy and ionic charge distributions. In order to finalize this work, a supplementary step where it is taken into account will be included to the analysis scheme. In addition, a re-analysis of the Exp.1 with updated tool and the construction of a reliable observable to rank the relative normalization possibilities are on going.

This work was supported by CEA, IN2P3 and “le défi NEEDS”. The authors are grateful for the support of the ILL and all the staff involved from CEA Cadarache and LPSC.

## Author contribution statement

The analyses and their comparison as well as the writing of this manuscript have been conducted by S. Julien-Laferrière and A. Chebboubi.

This work was supported and supervised by G. Kessedjian and O. Sero, who participated to the elaboration of the method and the preparation of the manuscript.

## References

1. H.G. Börner, F. Gönnerwein, *The Neutron* (World Scientific Publishing, Singapore, 2012)
2. N. Terranova et al., *Ann. Nucl. Energy* **109**, 469 (2017)
3. A. Plompen et al., *Eur. Phys. J. A* (to be submitted)
4. M.B. Chadwick et al., *Nucl. Data Sheets* **112**, 2887 (2011)
5. O. Serot et al., *Nucl. Data Sheets* **119**, 320 (2014)
6. P. Armbruster et al., *Nucl. Instrum. Meth.* **139**, 213 (1976)
7. H.R. Faust et al., ILL Internal Scientific Report 81FA45S, 1981
8. F. Martin, Ph.D. Thesis, Université de Grenoble, 2013
9. S. Julien-Laferrière et al., *EPJ Web Conf.* **169**, 00008 (2018)
10. H.R. Faust, Z. Bao, *Nucl. Phys. A* **736**, 55 (2004)
11. J.G. Heinrich, Report 6576, University of Pennsylvania, 2003
12. U. Köster et al., *Nucl. Instrum. Methods A* **613**, 363 (2010)
13. Y.K. Gupta et al., *Phys. Rev. C* **96**, (2017)
14. A. Bail, Ph.D. Thesis, Université Bordeaux I, 2009
15. A. Chebboubi, Ph.D. Thesis, Université de Grenoble-Alpes, 2015
16. M. Schmelling, *Phys. Scr.* **51**, 676 (1995)
17. A.C. Aitken, *Proc. R. Soc. Edin. A* **55**, 42 (1935)
18. A. Kessy, A. Lewin, K. Strimmer, *Am. Stat.* (2018), DOI: [10.1080/00031305.2016.1277159](https://doi.org/10.1080/00031305.2016.1277159)
19. B. Voirin et al., *EPJ Nuclear Sci. Technol.* **4**, 26 (2018)
20. F. Martin et al., *Nucl. Data Sheets* **119**, 328 (2014)